Structure of Ribonuclease A: Results of Joint Neutron and X-ray Refinement at 2.0-Å Resolution†

Alexander Wlodawer* and Lennart Sjölin‡

ABSTRACT: The structure of ribonuclease A has been refined jointly with the neutron and X-ray data extending to 2.0 Å. The results of an earlier X-ray refinement provided the starting model [Wlodawer, A., Bott, R., & Sjölin, L. (1982) *J. Biol. Chem. 257*, 1325–1332]. The final *R* factors were 0.159 (X-ray) and 0.183 (neutron) for a model containing all of the atoms expected in the protein, 128 waters, and a phosphate molecule in the active site. The joint refinement necessitated modifications in the orientation of a number of side chains, including the catalytically active lysine-41, which is now thought to form a salt link to the phosphate. Major modifications of the previous model of the bound solvent were necessary. The refinement of all atom occupancies with the neutron data only provided the information about the amide hydrogen exchange. A fourth of all amide hydrogens were found to be at least partially protected from exchange after a year of exchange with D_2O.

The crystal structure of bovine pancreatic ribonuclease (RNase) has been investigated with X-ray diffraction techniques by several groups. Recently the results of two independent refinements have been published. The diffraction data extending to 2.0 Å have been utilized by Wlodawer et al. (1982), while Borkakoti et al. (1982) used data extending to 1.45 Å. The starting point of both refinements was the structure partially refined at 2.5 Å by Wlodawer (1980). In addition, the structures of several complexes of inhibitors with ribonuclease, and of the native enzyme at cryogenic temperatures, have been refined by W. Gilbert and G. Petsko (unpublished results).

One of the drawbacks of the protein structural models based on X-ray diffraction by crystals is that, in the absence of very high resolution data (on the order of 1 Å), the positions of hydrogen atoms can be established only indirectly, on the basis of expected stereochemistry, rather than from observation. Such limitation is not present in the case of neutron diffraction, since the neutron scattering lengths of hydrogen and deuterium are comparable to those for nitrogen, oxygen, and carbon. Careful neutron diffraction experiments can unambiguously determine protonation states of important residues such as histidine in trypsin (Kossiakoff & Spencer, 1980, 1981) or in myoglobin (Phillips & Schoenborn, 1981; Hanson & Schoenborn, 1981). The orientation of side chains such as histidine, glutamine, and asparagine can be found with a high degree of confidence, based on the difference in the scattering of nitrogen, oxygen, and carbon and/or of attached hydrogens. In addition, neutron diffraction data can provide information about hydrogen exchange that is completely unavailable in the X-ray models. Since most experiments are performed in deuterated media, solvent scattering is more prominent and its structure easier to interpret.

Another reason for combining the results of X-ray and neutron diffraction experiments was discussed by Wlodawer & Hendrickson (1982). Since both types of data result from the same crystal structure, the number of observations can be increased by combining the two types of information in the same refinement. This can lead to a better overall description of the structure, due to the improvement of the ratio of observations to parameters. The influence of systematic errors can also be reduced, since they are unlikely to be similar in the two types of data.

In this paper we will describe the ribonuclease A structural model based on the results of joint refinement of X-ray and neutron data extending to 2.0-Å resolution. Preliminary results of the neutron studies at 2.8 Å have been published previously (Wlodawer, 1980; Wlodawer & Sjölin, 1981). Preliminary results of the amide hydrogen exchange investigation are also available (Wlodawer & Sjölin, 1982).

Experimental Procedures

The details of the procedures followed in this work have been described previously (Wlodawer, 1980; Wlodawer & Sjölin, 1982). Ribonuclease A crystals (space group $P2_1$, a = 30.18 Å, b = 38.4 Å, c = 53.32 Å, β = 105.85°) were grown at pH 5.3 from unbuffered protein solution with 43% *tert*-butyl alcohol as a precipitant. A number of crystals reached volumes of between 25 and 35 mm^3, with the largest crystal growing to 100 mm^3. The crystals grew as thick plates, with the shortest dimension along a^* not exceeding 1.5 mm. The crystals were deuterated by slow exchange of the original solution for a synthetic, fully deuterated mother liquor containing 55% deuterated *tert*-butyl alcohol (d_{10}; Aldrich) and 45% D_2O (99.8% D; Aldrich). The pH of this solution was adjusted to 5.25 with sodium deuteroxide (uncorrected pH meter reading). Several complete exchanges of the solvent took place in about 6 months. A crystal used for neutron data collection measured about 6 × 5 × 1 mm and was mounted in a quartz tube with its shortest dimension parallel to the tube axis. It was immersed in the mother liquor solution and immobilized with quartz wool. Three crystals which were used for X-ray data collection were fragments cut from larger crystals and were treated in the same way as the crystal used for neutron diffraction. They were mounted in 1-mm glass capillaries in the usual way.

Neutron data were collected by using the flat-cone diffractometer (Prince et al., 1978) located at the National Bureau of Standards Reactor. The neutrons were mono-

† From the National Measurement Laboratory, National Bureau of Standards, Washington, DC 20234, and the Laboratory of Molecular Biology, National Institute of Arthritis, Diabetes, and Digestive and Kidney Diseases, Bethesda, Maryland 20205. *Received November 2, 1982.*

* Address correspondence to this author at the National Measurement Laboratory, National Bureau of Standards.

‡ Present address: Department of Inorganic Chemistry, Chalmers Institute of Technology, Gothenburg, Sweden.

chromatized by reflection from a 50 × 100 mm graphite crystal that had a mosaic spread of 40 min. The wavelength of the neutrons was 1.68 Å. The neutron flux, measured in the sample position with a calibrated fission monitor, was 6 × 10^6 neutrons cm^{-2} s^{-1} (estimated error ±10%). The diffractometer was equipped with a linear position-sensitive detector 1 m long, mounted vertically on the counter arm. The neutron diffraction data set was collected in two parts. First, the diffractometer was used in equatorial geometry, neglecting intensities falling outside of the equatorial plane of the instrument. The reflections were measured by an ω step-scan method, with 64 steps counted every 0.025° (total width 1.6°). The time spent counting each reflection was 10 min for the resolution up to 3.2 Å and 20 min in the shell between 3.2 and 2.8 Å. These times are approximate since the counting periods were based on the output of a low-efficiency main-beam monitor, which compensated for the flux instability. Data were corrected for absorption (North et al., 1968), but the influence of neutrons with half-wavelengths was neglected.

Another data set extending to 2.0-Å resolution for the level $h = 0$ and somewhat higher resolution for the upper levels was collected in flat-cone geometry. In this mode the crystal was rotated around its a axis while the data for one level were measured. Next, the detector was moved to a position appropriate for a new level, and the process was repeated. Altogether data from 16 levels (h = 0–15) were collected. Since a complete 360° ψ scan was performed for each level (in 0.09° steps, counting time approximately 50 s/step), each accessible reflection was counted at least twice. The reflection intensities were integrated by using the dynamic mask procedure (Sjölin & Wlodawer, 1981), which improved the precision of the data and increased the number of statistically significant structure amplitudes [$I > 3\sigma(I)$]. The absorption correction was initially applied by the method of Santoro & Wlodawer (1980), but its influence was so small that it was later disregarded. Again, no correction for the $\lambda/2$ wavelength was applied.

The data measured in the equatorial and flat-cone geometries were merged together by using the scaling algorithm of Hamilton et al. (1965). The combined data set did not have any blind regions, inherent if a crystal is rotated around a single axis in the flat-cone geometry. The scaling R factors ($R_{sca} = \sum|F_1 - sF_2|/\sum F_1$, where F_1 and F_2 represented the structure amplitudes measured in the equatorial and flat-cone geometries, respectively) varied from 0.055 to 0.071 for levels 0–8 (Sjölin & Wlodawer, 1981). The total number of reflections considered to be observed in the 2–10-Å shell was 4132 (51% of the theoretical maximum).

The X-ray data set extending to 2.0-Å resolution was collected with three crystals on a Picker FACS-1 diffractometer controlled by a PDP8/I computer and VANDY operating system (Lenhert, 1975). The diffractometer was operated in the ω step-scan mode, with the total scan width between 0.6° and 0.75°, covered in 13, 19, or 26 steps. The reflections were integrated by summing the 7, 11, and 14 highest contiguous steps, respectively, while the other points in the profile were used to determine the individual background for each reflection. Counting time per reflection varied between 39 and 52 s for different crystals. A linear decay correction was applied on the basis of three standard reflections monitored every 100 reflections (maximum correction 1.18). Absorption correction was applied by the method of North et al. (1968). The number of observed reflections in the 10–2-Å shell was 7708, 95.6% of the theoretical maximum. This data set has been previously used in the X-ray refinement of ribonuclease A at 2.0-Å resolution (Wlodawer et al., 1982).

The lists of the final structure factors, both neutron and X-ray, have been deposited at the Brookhaven Protein Data Bank. The refined coordinates were also deposited.

Computational Procedures

The computational procedure for the joint protein structure refinement with the X-ray and neutron data was used for ribonuclease refinement. This procedure was described in detail by Wlodawer & Hendrickson (1982). It required relatively minor conceptual modifications to the stereochemically restrained refinement procedures (Hendrickson & Konnert, 1981) that were previously used to refine the structure of ribonuclease A with the X-ray data (Wlodawer et al., 1982). The principal modifications enabled hydrogens to be included in the model, with separate scattering lengths for H and D atoms. The X-ray and neutron diffraction data had separate weights, but otherwise all diffraction data, together with stereochemical restraint information, were used to calculate a single matrix. Amino acid standard groups that contained hydrogen positions were prepared on the basis of neutron structures whenever available. The contribution of hydrogen atoms was neglected in the calculation of X-ray scattering factors, while their positions were identified as either H or D for the choice of appropriate scattering length in the neutron calculations. The version of the program used for full structure refinement did not allow variable hydrogen/deuterium occupancy ratios. A separate version was therefore used to refine these occupancies. This special version of the refinement program allowed the occupancies for all atoms (and not only the hydrogens) to vary and was run only to refine the occupancies (that is, without allowing the positional and thermal parameters to vary; Wlodawer & Sjölin, 1982).

Difference Fourier maps were examined by using interactive computer graphics. The program FRODO (Jones, 1978), implemented on the VAX11/780 for the Evans and Sutherland Multi-Picture System by B. Bush, allowed us to manipulate the model and to fit it to density maps. The difference Fourier maps were usually calculated with either X-ray or neutron coefficients of the type $2F_o - F_c$. For some regions where the structure was more seriously in doubt, the maps were sometimes calculated with the coefficients $F_o - F_c$ after the contribution of a portion of the atoms to structure factor calculations was subtracted. Such "fragment ΔF" maps were expected to show less refinement-induced bias.

Results

Structure Refinement and Rebuilding. The initial model of RNase was reasonably well refined, with the crystallographic R factor of 0.159 for the X-ray data within the 10–2-Å resolution limits. The model included all atoms expected to belong to the protein chain, as well as a phosphate molecule bound near the active site and 176 water molecules, many of them with fractional occupancies. While the starting model was based mainly on the X-ray refinement, an exception was that the orientation of the four histidine side chains was previously determined on the basis of neutron difference Fourier maps calculated with 2.8 Å data (Wlodawer & Sjölin, 1981). The neutron R factor for the initial model was 0.32, lowered to 0.306 by the addition of hydrogens in positions predicted by stereochemistry.

Several changes were indicated by inspection of the neutron difference Fourier maps in the course of the present refinement. Eight amino groups belonging to the asparagine and glutamine side chains had to be rotated by 180° in order to

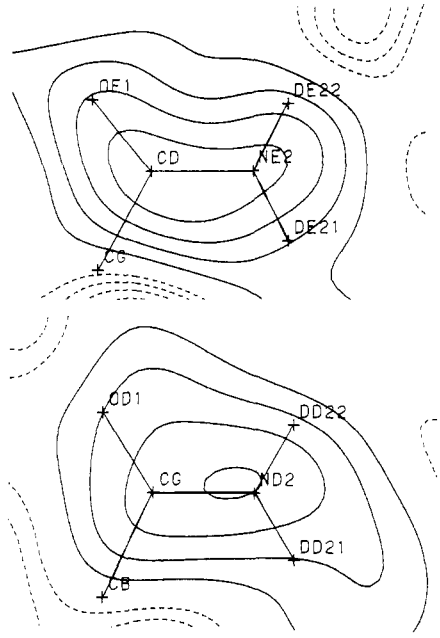

FIGURE 1: Section through a neutron ($2F_o - F_c$) difference Fourier map for the side chains of Gln-74 (top) and Asn-94 (bottom). Positive contours (solid) correspond to 1 F level and negative contours (dashed) to 0.5 F. The atomic coordinates of the final model are superimposed on the map.

agree with the respective maps (Figure 1). The affected side chains were Asn-24, -27, -44, -71, -94, and -103 and Gln-69 and -74. The differences between the neutron scattering of a single oxygen atom and a ND_2 group are very large (a factor of 3.5), and an indication of such reorientation is usually easy to notice. This is unlike the X-ray case, where very high resolution data are necessary for this purpose.

Another residue which required a turn of the side chain was Thr-99. The positions of CG2 and OD1 were exchanged by rotation of the side chain by 180°. This change was also made primarily in order to satisfy the neutron map, since the bend in the X-ray map was not clear enough to make the assignment unambiguous. Similarly, the carboxyl terminus was switched with the side chain of Val-124 in order to satisfy the neutron maps.

The position of the Arg-39 side chain was completely altered, since the initial orientation corresponded to a rather weak density and a much better density was found nearby. A section of a neutron difference Fourier map of the guanidinium group is shown in Figure 2, and a reasonably good agreement can be noticed.

In the final model, the orientation of His-105 is reversed compared to the assignment resulting from the 2.8-Å neutron refinement (Wlodawer & Sjölin, 1981). The original assignment was derived by the fitting of the difference Fourier map and was not supported by additional information such as hydrogen bonding, since all potential hydrogen bonds involving the imidazole ring atoms were too long. The subsequent refinement, however, showed a proper distance from the carbonyl oxygen of Ser-75 to the imidazole, but only if the orientation of the ring was changed. While the difference Fourier map supported the then current orientation, the refinement of atomic occupancies (see below) indicated that the hydrogens and deuteriums of the ring should change the signs of scattering lengths, thus supporting the suggested change. Nevertheless, the fragment ΔF map of His-105 was rather ambiguous, both before and after reorientation of this residue. We have finally decided to reorient His-105, while it is still possible that both orientations are present in the crystals.

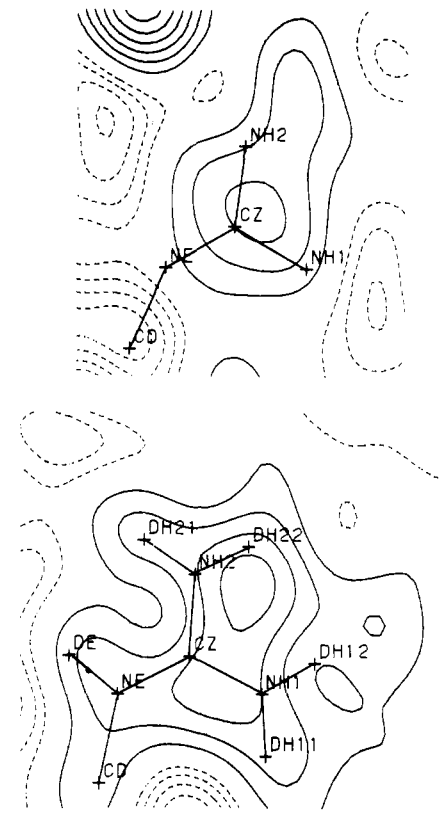

FIGURE 2: Sections through a neutron ($2F_o - F_c$) difference Fourier map of Arg-39, contoured as in Figure 1. (Top) Starting model, superimposed on the corresponding difference map. (Bottom) Final map and model after reorientation. The improvement in the fit is obvious.

The positions of two lysine side chains (Lys-7 and Lys-37) were substantially modified in the course of the refinement (without manual intervention). The presumable reason is that the strong scattering of a ND_3 group is a better marker for the end of this side chain in the neutron than in the X-ray diffraction, and thus the joint refinement carried more information about the exact positioning of these side chains. Even more telling is the case of the catalytically important Lys-41, which we originally placed with the terminal nitrogen NZ 9.4 Å from the phosphorus and 8.27 Å from the oxygen O4 of the phosphate. We realized that an alternate position was possible, but the Fourier map was quite ambiguous (Figure 3a). On the other hand, an unexplained density could be seen near the phosphate in the corresponding neutron map (Figure 3b), and we attempted to manually change the orientation of this side chain in such a way as to place the terminal NZ and associated deuterium atoms in that density. This tentative model was later refined, and the resulting X-ray and neutron Fourier maps proved the new orientation to be correct (Figure 3c,d). It is somehow disconcerting that the proper positioning of this side chain would change the maps (which were calculated without the use of Lys-41 coordinates in the phasing) to such an extent. For this residue the availability of maps calculated with the two types of radiation data was clearly beneficial.

The final model resulting from the joint refinement was characterized by R factors of 0.159 (X-ray) and 0.183 (neutron). Thus the X-ray R factor was unchanged by the refinement procedure. The bond lengths differed from the ideal values by 0.023 Å. The overall root mean square discrepancy between the positions of all nonhydrogen, nonsolvent atoms in the X-ray and joint refinement models was 0.70 Å, and the discrepancy between the temperature factors was 1.3 Å^2. The

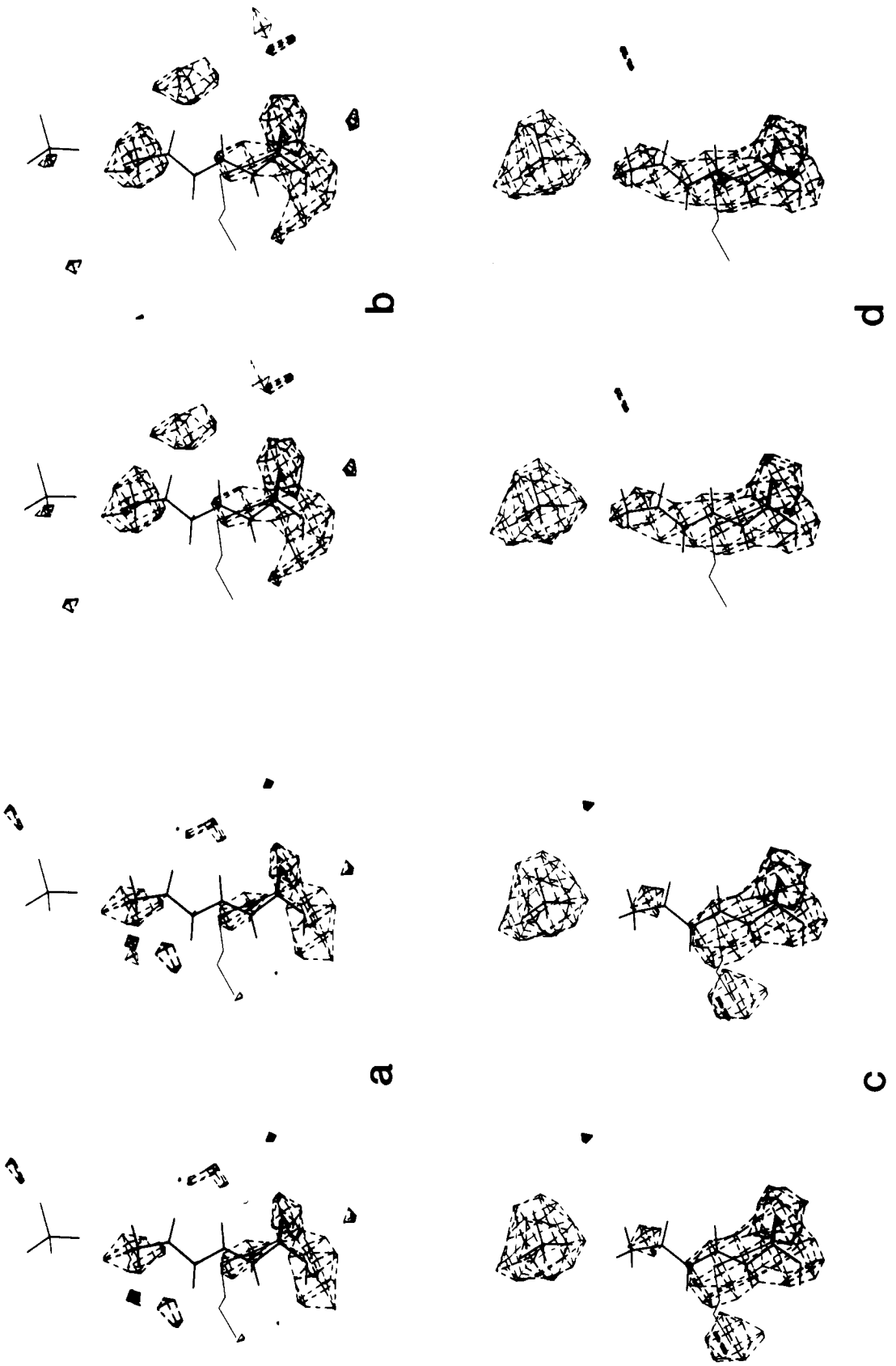

FIGURE 3: Fragment ΔF difference Fourier maps for Lys-41, calculated on the basis of models excluding the coordinates of this side chain, of water 152, and of the phosphate from phase calculations. Initial (X-ray) coordinates of Lys-41 in thin line; final coordinates (joint refinement) in bold line. The contours are at $+2\sigma$ level only. (a) Neutron data, initial model; (b) neutron data, final model; (c) X-ray data, initial model; (d) X-ray data, final model.

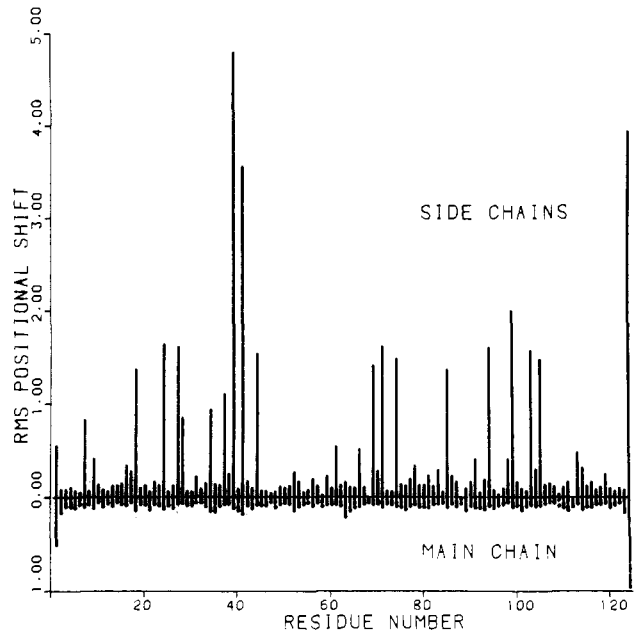

FIGURE 4: Root mean square positional shifts between the atomic positions in the initial and the final models (in Å). The shifts are plotted separately for the atoms belonging to the main chain (lower plot) and to the side chain (upper plot).

distributions of the discrepancies calculated separately for the main-chain and side-chain atoms of each residue is shown in Figure 4. It is clear that the changes to the main-chain coordinates were very minor, and those for the side-chain atoms were mostly limited to those discussed above. After removing the side-chain amides, carboxyl terminus, and complete side chains of Lys-7, Ser-18, Lys-37, Arg-39, Lys-41, His-105, and Val-124, the remaining root mean square discrepancy was only 0.19 Å. This compares well with the estimate of the standard deviations in the atomic positions made on the basis of the plot of X-ray R factors vs. resolution (Luzzati, 1952), which yielded an estimate of $\Delta r = 0.17$ Å. Thus we may conclude that the inclusion of neutron data in the refinement did not change the average atomic positions by more than their estimated standard deviations, with the exception of those atoms which had to be drastically altered.

Solvent Structure. The ribonuclease model based on the X-ray refinement contained 176 water sites, many of them only partially occupied. The criterion for deciding whether a given feature in a map corresponded to a solvent molecule or to noise was the presence of unambiguous and persistent density and stable behavior during the refinement. This model was then used as a starting point for the joint neutron/X-ray refinement after deuterium atoms were added to the oxygens to form D_2O molecules with standard bond lengths and angles. The waters were initially oriented by using computer graphics and a neutron difference Fourier map. In frequent cases when the map carried little information about the preferred orientation of deuterium, we tried to satisfy the most probable hydrogen bonds. These models were subsequently subjected to the joint refinement, and the process of map examination was repeated. Those solvent molecules whose occupancies dropped drastically during the refinement, or for which either the electron or the nuclear density was missing, were removed. The coordinates for waters 133, 136, 161, 203, 215, 235, and 249 were replaced by their symmetry equivalents in order to be more consistent with the numbering of the parts of the protein in their vicinity. Several difference Fourier maps were calculated at various stages of refinement in order to look for water molecules not present in the original model. These "new" waters were evaluated with the same criteria. The final model of the solvent consisted of 128 sites (Figure 5), 117 of which were derived from the original model and the remaining ones were new. The root mean square displacement of the oxygen positions for the common sites was 0.60 Å, while the root mean square change in the temperature factors was 10 Å^2 and the root mean square change in occupancies, 0.18. Clearly, the new model of the solvent structure was a serious departure from the original.

Hydrogen Bonds. (*a*) *Intramolecular Hydrogen Bonds.* A schematic diagram showing the hydrogen bonds between the main-chain atoms is shown in Figure 6. These assignments are almost unchanged compared with the results of the X-ray refinement (Wlodawer et al., 1982). The hydrogen bonds which were deleted in the current diagram were those between the amide nitrogen of Met-31 and the carbonyl of Asp-27 (bond too long, N···O distance 3.53 Å), as well as those between N-16–O-14 and N-113–O-114 (N–H–O angles 100° and 60°, respectively). The bonds added to the diagram were those between N-95 and O-93 and between N-119 and O-109. The bond between N-58 and O-55 (3_{10} helix), which was considered to be long before and was therefore dashed, is now closer to the standard length and is marked solid. These changes emphasized the distortions of the helix H2 (residues 24–34) and the transition from the α-helix to the 3_{10} helix in the helix H3 (residues 50–60) but otherwise did not lead to any modification of the secondary structure of RNase, which seems to be very well established now.

A complete list of all intramolecular hydrogen bonded interactions (including the solvent) is presented in Table I of the supplementary material (see paragraph at end of paper

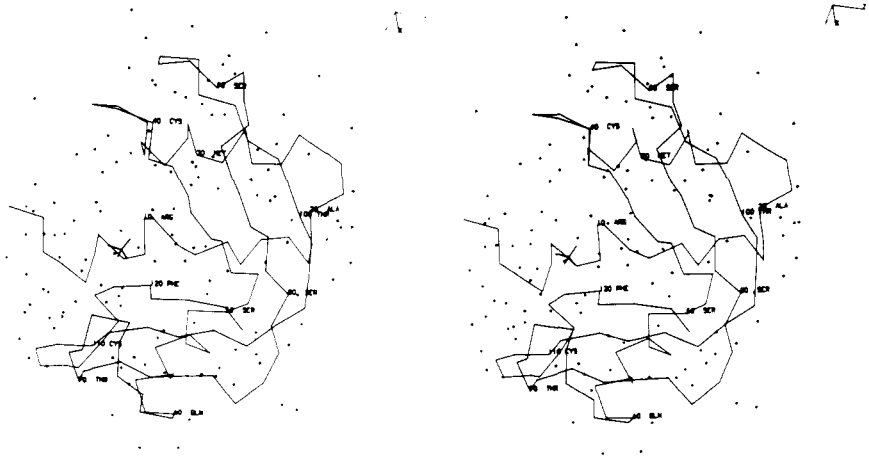

FIGURE 5: C_α tracing of the main chain of ribonuclease A, with the positions of water molecules and the phosphate superimposed.

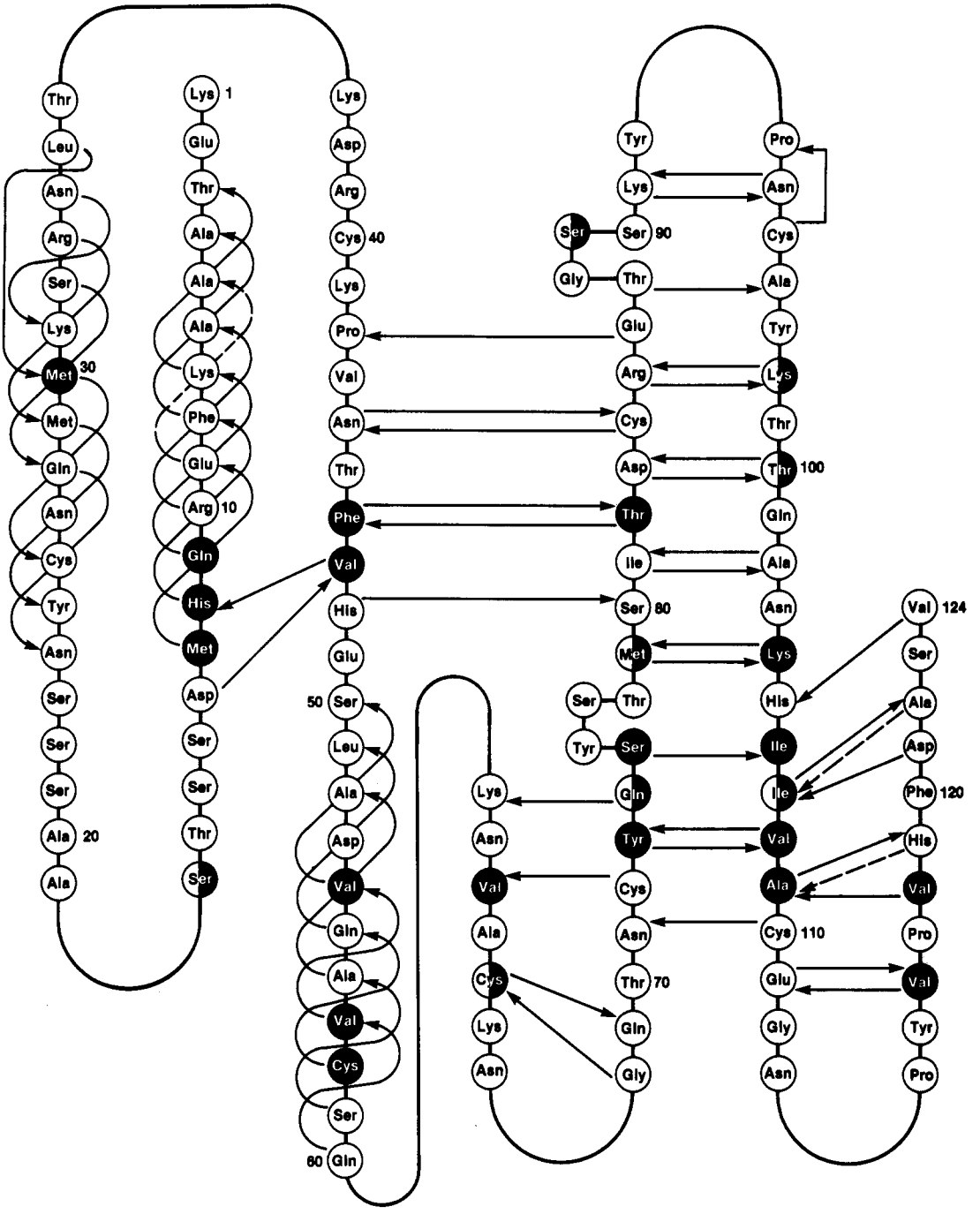

FIGURE 6: Diagram of hydrogen bonds involving the main-chain atoms and the level of protection of amide hydrogens. Bonds shorter than 3.15 Å are solid, and those between 3.15 and 3.35 Å and with expected angles are dashed. Filled circles correspond to fully protected amide hydrogens and half-filled circles to partially protected. (For details, see the text.)

regarding supplementary material). Many of the interactions involving the side-chain groups and the solvent have changed as a result of the joint refinement, due to the reorientation of many side-chain amino groups and to repositioning the solvent. It is possible that other solvent molecules, in addition to those listed in Table I of the supplementary material, are also involved in hydrogen bonds, since many waters can probably be found in multiple orientations. Such possibilities, however, were not considered in the refinement in view of the moderate resolution of the diffraction data.

(*b*) *Intermolecular Hydrogen Bonds.* The number of hydrogen bonds between the neighboring molecules in the crystal is small (Table II of the supplementary material). Only four direct contacts between the peptide atoms can be observed. The interaction between NH1 of Arg-39 and OE1 of Glu-111 was not previously reported since it results from the major redefinition of the position occupied by the side chain of arginine-39. In addition, a number of intermolecular bridges are provided by water molecules. The small number of intermolecular hydrogen-bonded interactions is important in interpreting the results of hydrogen-exchange data (see below), since it is unlikely that so few interactions could seriously modify the flexibility and accessibility to solvent of different parts of the secondary structure of RNase, compared to the situation existing in solution.

Hydrogen Exchange. The information about amide hydrogen exchange, not available in the X-ray structure determination, becomes accessible during analysis of the neutron data. This happens because the crystals are usually soaked in deuterated mother liquor before neutron data are collected

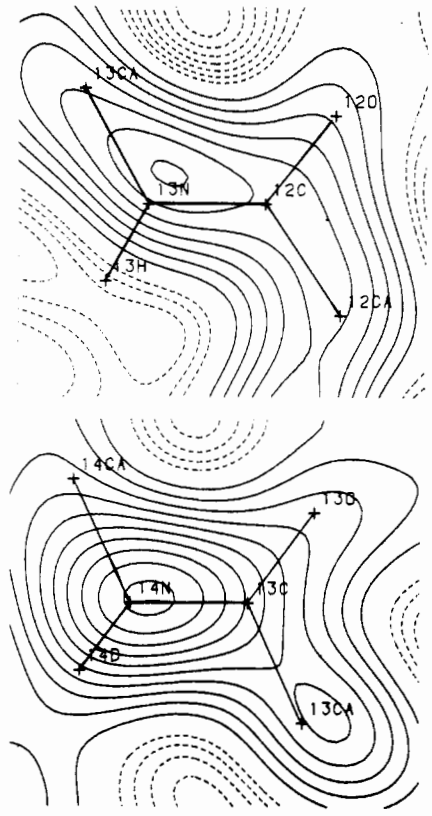

FIGURE 7: Sections through a neutron ($2F_o - F_c$) difference Fourier map, contoured at +0.5 F (solid lines) and at −0.25 F (dashed lines). (Top) Amide of Met-13, fully protected from exchange. (Bottom) Amide of Asp-14, fully exchanged.

in order to reduce the incoherent background caused by the presence of hydrogen atoms in the protein. The time required for the exchange of unprotected amide hydrogens is much less than the several months usually spent on solvent exchange, while the most highly protected amides can stay unexchanged longer than that (Rosa & Richards, 1981; Kossiakoff, 1982). While such neutron diffraction experiments cannot provide direct kinetic information about the exchange processes, they can pinpoint the nonexchangeable sites without ambiguity.

The methods used in the evaluation of hydrogen exchange in ribonuclease A were detailed previously (Wlodawer & Sjölin, 1982) and will not be discussed here. The final estimates of the occupancies of amide hydrogens were obtained in a neutron refinement in which all atomic parameters other than the occupancies were held constant, while the occupancies of all atoms were allowed to vary. A maximum occupancy of 1.0 was enforced for all atoms other than amide hydrogens, for which no limits were placed on the occupancies. Initially all amide hydrogens were assigned as deuterium with an occupancy of 1.0, and in the ideal case, the occupancies of nonexchangeable hydrogens should become −0.55 (based on the magnitude and the sign of scattering length of H and D). The scatter of occupancies beyond these limits would be caused by the errors in the procedure, while the H/D ratios could be calculated for those amide hydrogens whose occupancies were within these limits. The error in the estimate of occupancies was found to be ±15%. The derived occupancies of amide hydrogens were further checked by the analysis of difference Fourier maps (Figure 7), which were found to be in generally good agreement with the refinement results.

The results found in this study differ slightly from those presented earlier (Wlodawer & Sjölin, 1982), since the starting model used for occupancy refinement was better than the one utilized previously. Nevertheless, only a few sites are affected (four of the sites previously considered half-exchanged are now fully exchanged), and the general conclusions drawn previously are still valid.

In view of the relatively large errors in the estimates of individual occupancies, the protected amides were divided into two classes. Nineteen amides were found to be fully protected (more than 80% H), and eight were partially exchanged (40–80% H). The protected amides are marked in Figure 6, which also shows the correlation between the positions of the protected amides within the peptide chain and between the elements of secondary structure. A vast majority (23 out of 27) of the protected amide hydrogens form hydrogen bonds to main-chain oxygen atoms in either helical or β-sheet secondary structures. However, the participation in such bonds is not a guarantee of protection, since almost two-thirds of the hydrogens involved in the main-chain hydrogen bonding network are fully exchanged. Of the remaining protected hydrogens, one is involved in an unambiguous hydrogen bond to the side-chain group and one forms a bond to a carbonyl oxygen in irregular secondary structure.

The distribution of protected amides in the ribonuclease structure is not uniform. Of the two distinct areas surrounding the cleft near the active site, one appears to be much more flexible than the other. In particular, the part of the β-sheet containing residues 63, 65, 73–75, 79, 104, 106–109, 116, and 118 appears to be much more highly protected from exchange than any other region of the protein. Only the central part of the β-sheet found in the other half of the molecule contains protected amides (46, 82, 98, and 100). Each of the helices contains at least one protected amide, but three amides in a row are protected only in the first helix. These amides (11–13) are located at the carboxyl end of the helix, near the active site cleft.

A calculation of the atomic surfaces accessible to solvent was performed with a program written by M. L. Connolly (unpublished results). In this calculation the atomic radius for hydrogen was assumed to be 1.27 Å, and the radius of a solvent probe was 1.4 Å. Altogether 77 amide hydrogens were calculated to have no exposed surfaces at all, while the exposed surfaces of the other 43 ranged from 0.5 to 11.3 Å^2 (Table III of the supplementary material). Two of the exposed amide hydrogens (18 and 89) appear to be partially protected in the neutron study, and this result is probably due to the errors in the refinement procedure. They represent less than 10% of the total number of protected amides, and such a number of potentially erroneous assignments is consistent with the estimated accuracy of the method.

The number of buried amides approaches two-thirds of the total (even though ribonuclease is rather small and, therefore, the fraction of surface residues is large), but only one-third of them are actually protected from exchange. It is not clear at this stage why some amides are much more highly protected than others, even though they are all found in quite similar environments, both in terms of the accessibility to the solvent and the type and number of strong hydrogen bonds which they make.

Kossiakoff (1982) postulated that the exchange behavior of amide hydrogens in trypsin could be best explained by a model involving "regional melting", usually limited to breaking only a small number of hydrogen bonds. This result was partially based on the observation that the protected amides in α-helices are scattered, and thus the cooperative unzippering of the whole helix is not necessary in order for the exchange to occur. The protected amides in the helical regions of trypsin

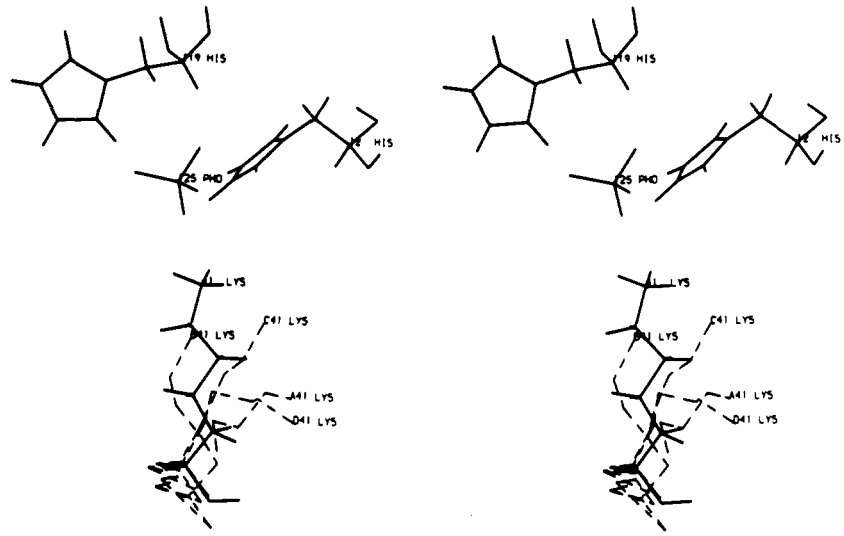

FIGURE 8: Part of the active site of RNase A. Positions of His-12, His-119, Lys-41, and the phosphates which were determined in this study are drawn solid. The coordinates taken from selected previous models of the orientation of Lys-41 are dashed. A41, refined RNase S (Powers, 1976); B41, unrefined RNase S (Wyckoff et al., 1970); C41, RNase A refined by Borkakoti et al. (1982); D41, RNase A refined by Wlodawer et al. (1982).

were found to be on the interfaces between the helices and β-sheets. Similar behavior can be noticed for two out of three helices present in ribonuclease (even though the protected, helical amide 30 is close to a regular β-sheet which apparently does not offer protection to its own amides). The helical amides 54, 57, and 58 are adjacent to the highly protected β-sheet region, and the same is true for the three consecutive amides (11–13) of the helix H1, which are found in direct contact with the protected area of a β-sheet. Only the behavior of the latter helix could be described by a total cooperative unzippering, as was done by Schreier & Baldwin (1976). More systematic analysis of the hydrogen-exchange properties of ribonuclease and their correlation with the dynamics of the molecule will require extensive modeling studies by using the exchange information reported here as a base.

Discussion

Joint refinement of the structure of ribonuclease with the X-ray and neutron data has resulted in a model which, while not vastly different from the previous one (Wlodawer et al., 1982), has nevertheless elucidated a number of features which were unclear. Of particular interest is the unambiguous placement of Lys-41 in the vicinity of the phosphate. Figure 8 shows a comparison of the positions assigned to this residue in some previous studies of ribonucleases A and S. RNase S coordinates were rotated into a RNase A cell as described before (Wlodawer et al., 1982). It can be seen that the positions of Lys-41 vary widely, as the orientations assigned previously were not based on unambiguous electron density. It is probably coincidental that the coordinates published in the original unrefined RNase S structure are the closest to the ones reported here. While the previous positioning of Lys-41 required large shifts of its side chain upon substrate binding if this residue were to play any catalytic role, the present model does not require such large shifts.

Combining the neutron and X-ray data in a joint refinement leads to an increase of the total number of observations, while the number of parameters is the same as in the separate neutron refinement. For the well-determined parts of the structure such as the main chain, the additional data seem to play a minor role, and the results of the joint refinement were virtually identical with the previous X-ray refinement (Figure 4). This is not true for those parts of the structure which were not determined so well. The inclusion of neutron data may lead to repositioning the amino acids directly in the refinement (such was the case for lysines-7 and -37), but the nature of the change required for other groups may be such as to preclude their automatic reorientation. In particular, the refinement is incapable of reorienting the terminal amino groups of glutamine and asparagine side chains, but the indication for the necessity of such changes can be provided by the difference Fourier maps. The shift which had to be applied to some other side chains (such as Lys-41 and Arg-39) was larger than the radius of convergence of the refinement, and manual intervention was also necessary.

The availability of the two types of maps was particularly important in our rebuilding of the structure of the solvent. About one-third of the sites reported on the basis of only X-ray data were removed from the joint refinement model for lack of corresponding nuclear densities. While the deuterium positions could be determined unambiguously for some of the most strongly bound waters, nuclear densities corresponding to the solvent were often featureless, and the orientation of such molecules was less certain. In particular, many water molecules were found in positions in which they could make more hydrogen bonds than the number of hydrogens available for this purpose, which may indicate either space- or time-averaged changes in hydrogen bonding.

The availability of neutron diffraction data provides a unique contribution to the determination of the exchange properties of amide hydrogens. The protected amides can be observed directly, with the uncertainty in the determination of the individual hydrogens of about 15%. The differences between the number of protected amides in the two halves of the β-sheet cannot be currently explained, but the distribution of the protected amides can serve as a starting point of the theoretical calculations.

Acknowledgments

We are grateful to Dr. D. Davies for his encouragement and support of this work and to Drs. W. Gilbert and G. Petsko for exchanging unpublished information throughout the duration of the project. We are indebted to Drs. L. Getzoff and J. Tainer for providing us with their results of the surface accessibility calculation for ribonuclease. Sheryl Long provided us with invaluable editorial assistance.

Supplementary Material Available

Complete lists of intramolecular (Table I) and intermolecular (Table II) hydrogen bond lengths and angles, as well as results of solvent accessibility calculations for amide hydrogens (Table III) (6 pages). Ordering information is given on any current masthead page.

Registry No. RNase A, 9001-99-4.

References

Borkakoti, N., Moss, D. A., & Palmer, R. A. (1982) *Acta Crystallogr., Sect. B B38*, 2210-2217.

Hamilton, W. C., Rollett, J. S., & Sparks, R. A. (1965) *Acta Crystallogr. 18*, 129-130.

Hanson, J., & Schoenborn, B. P. (1981) *J. Mol. Biol. 153*, 117-146.

Hendrickson, W. A., & Konnert, J. H. (1981) in *Biomolecular Structure, Conformation, Function, and Evolution* (Srinivasan, R., Ed.) Vol. 1, pp 43-57, Pergamon Press, Oxford.

Jones, T. A. (1978) *J. Appl. Crystallogr. 11*, 268-272.

Kossiakoff, A. A. (1982) *Nature (London) 296*, 713-721.

Kossiakoff, A. A., & Spencer, S. A. (1980) *Nature (London) 288*, 414-416.

Kossiakoff, A. A., & Spencer, S. A. (1981) *Biochemistry 20*, 6462-6474.

Lenhert, P. G. (1975) *J. Appl. Crystallogr. 8*, 568-570.

Luzzati, V. (1952) *Acta Crystallogr. 5*, 802-810.

North, A. C. T., Phillips, D. C., & Mathews, F. S. (1968) *Acta Crystallogr., Sect. A A24*, 351-359.

Phillips, S. E. V., & Schoenborn, B. P. (1981) *Nature (London) 292*, 81-82.

Powers, T. B. (1976) Ph.D. Thesis, Yale University.

Prince, E., Wlodawer, A., & Santoro, A. (1978) *J. Appl. Crystallogr. 11*, 173-178.

Rosa, J. J., & Richards, F. M. (1981) *J. Mol. Biol. 145*, 835-851.

Santoro, A., & Wlodawer, A. (1980) *Acta Crystallogr., Sect. A A36*, 442-450.

Schreier, A. A., & Baldwin, R. L. (1976) *J. Mol. Biol. 105*, 409-426.

Sjölin, L., & Wlodawer, A. (1981) *Acta Crystallogr., Sect. A A37*, 594-604.

Wlodawer, A. (1980) *Acta Crystallogr., Sect. B B36*, 1826-1831.

Wlodawer, A., & Sjölin, L. (1981) *Proc. Natl. Acad. Sci. U.S.A. 78*, 2853-2855.

Wlodawer, A., & Hendrickson, W. A. (1982) *Acta Crystallogr., Sect. A A38*, 239-247.

Wlodawer, A., & Sjölin, L. (1982) *Proc. Natl. Acad. Sci. U.S.A. 79*, 1418-1422.

Wlodawer, A., Bott, R., & Sjölin, L (1982) *J. Biol. Chem. 257*, 1325-1332.

Wyckoff, H. W., Tsernoglou, D., Hanson, A. W., Knox, J. R., Lee, B., & Richards, F. M. (1970) *J. Biol. Chem. 245*, 305-328.

Plasma Actin Depolymerizing Factor Has both Calcium-Dependent and Calcium-Independent Effects on Actin†

Harriet E. Harris and Alan G. Weeds*

ABSTRACT: The effects of pig plasma actin depolymerizing factor (ADF) on both G-actin polymerization and F-actin fragmentation have been examined by using rabbit skeletal muscle actin labeled with *N*-(1-pyrenyl)iodoacetamide, a sensitive fluorescent probe for monomer to filament interconversion. Fluorescence data have been compared with results obtained by viscometry and by difference absorption measurements at 232 nm. Plasma ADF nucleates actin filament assembly in a Ca^{2+}-dependent manner; actin polymerization rates are enhanced at greater than 10^{-6} M Ca^{2+}. The calcium concentration dependence of this effect, showing a shift in ADF nucleating capacity between 10^{-6} and 10^{-7} M Ca^{2+}, is that expected for an intracellular regulatory effect, but in plasma, the protein would always be saturated with Ca^{2+}. Although the rate of polymerization is markedly enhanced in the presence of calcium ions, the extent of polymerization (as determined by the amplitude of the fluorescence change or the specific viscosity) is reduced in the presence of ADF and shows little or no Ca^{2+} dependence. The critical concentration of actin monomers is increased in the presence of ADF whether calcium is present or not. When ADF is added to F-actin, there is an immediate fall in fluorescence. This conversion of filaments to monomers by ADF (as defined by the fluorescence changes) is unaffected by calcium concentration. Electron micrographs of F-actin treated with ADF show that the filaments are indeed shortened at both high and low calcium concentrations. Taken together, these observations are interpreted in terms of a model in which ADF has both Ca^{2+}-sensitive and Ca^{2+}-insensitive binding sites for actin.

Plasma actin depolymerizing factor (ADF)[1] is a protein which disrupts actin filaments and is found in relatively large amounts in plasma and serum from a variety of species (Norberg et al., 1979; Chaponnier et al., 1979; Harris et al., 1980; Harris & Schwartz, 1981). Filament fragmentation has been observed by electron microscopy and monitored by viscosity and sedimentation studies. In addition, the DNase inhibition assay has shown that ADF acts rapidly on actin

† From the MRC Laboratory of Molecular Biology, University Medical School, Cambridge CB2 2QH, U.K. *Received August 3, 1982.*

[1] Abbreviations: ADF, plasma actin depolymerizing factor; PMSF, phenylmethanesulfonyl fluoride; DTT, dithiothreitol; EGTA, ethylene glycol bis(β-aminoethyl ether)-*N*,*N*,*N*′,*N*′-tetraacetic acid; $NaDodSO_4$, sodium dodecyl sulfate; Tris, tris(hydroxymethyl)aminomethane; Bicine, *N*,*N*-bis(2-hydroxyethyl)glycine.

0006-2960/83/0422-2728$01.50/0